# Phototransistor-based optoelectronic tweezers for dynamic cell manipulation in cell culture media†

Hsan-yin Hsu,*[a] Aaron T. Ohta,*[b] Pei-Yu Chiou,*[c] Arash Jamshidi,[a] Steven L. Neale[a] and Ming C. Wu[a]

*Received 14th April 2009, Accepted 5th August 2009*
*First published as an Advance Article on the web 7th September 2009*
**DOI: 10.1039/b906593h**

Optoelectronic tweezers (OET), based on light-induced dielectrophoresis, has been shown as a versatile tool for parallel manipulation of micro-particles and cells (P. Y. Chiou, A. T. Ohta and M. C. Wu, *Nature*, 2005, **436**, 370–372).[1] However, the conventional OET device cannot operate in cell culture media or other high-conductivity physiological buffers due to the limited photoconductivity of amorphous silicon. In this paper, we report a new phototransistor-based OET (Ph-OET). Consisting of single-crystalline bipolar junction transistors, the Ph-OET has more than 500× higher photoconductivity than amorphous silicon. Efficient cell trapping of live HeLa and Jurkat cells in Phosphate Buffered Saline (PBS) and Dulbecco's Modified Eagle's Medium (DMEM) has been demonstrated using a digital light projector, with a cell transport speed of 33 μm/sec, indicating a force of 14.5 pN. Optical concentration of cells and real-time control of individually addressable cell arrays have also been realized. Precise control of separation between two cells has also been demonstrated. We envision a new platform for single cell studies using Ph-OET.

## Introduction

Manipulation of individual cells has many applications in fundamental research and biomedicine. For example, the precise control of cellular location facilitates the investigation of cell behaviors such as cell-to-cell and cell-to-environment interactions. It is also useful in sample preparation protocols, such as sample sorting and concentrating. Some widely used non-invasive cell manipulation techniques include optical tweezers[2,3] and electrode-based dielectrophoresis (DEP).[4–7] Optical tweezers use tightly focused optical beams to trap particles through the gradient of the optical field.[2] It requires high optical intensity and tight optical focusing. A typical optical trap requires a laser intensity of $1 \times 10^6$ W/cm$^2$, which may cause optical or thermal damage to the biological specimens.[8,9] Furthermore, the high numerical aperture objective lens required for tight focusing limits the field of view and the number of optical traps. On the other hand, DEP utilizes the interaction of a particle's induced dipole with a non-uniform electric field.[10] The non-uniform electric fields are typically generated by microfabricated electrodes. DEP provides high throughput, however it lacks the flexibility of dynamic control since fixed electrodes are used.

Optoelectronic tweezers[1,11,12] (OET) address the limitations of optical tweezers and electrode-based DEP. Utilizing optically-induced DEP, OET retains the flexibility of optical tweezers, while offering increased parallel manipulation capabilities. Up to 15 000 individually-addressable traps have been generated over an area of 1 mm$^2$. A typical OET trap requires 10 000× less optical intensity compared to optical tweezers, enabling us to use a simple digital light projector to simultaneously control a large number of traps. OET has been used for trapping polystyrene particles,[1,11] metallic and semiconducting nanowires,[13] DNA,[14,15] and biological cells.[1] Various other devices with enhanced functionalities have also been developed based on the OET principle, including the lateral-field OET for manipulation of nanowires[16,17] and microdisks,[18] the double-photoconductive-layer OET device for 3-D particle manipulation,[19] and floating electrode OET for droplet manipulation in oil.[20] OET can also be integrated with a liquid-crystal display (LCD) to eliminate projection optics,[21,22] providing a miniaturized cell and particle manipulation platform. Based on the OET platform, light addressable *in-situ* cell electroporation[23] and cell lysis[24] have also been demonstrated.

However, the conventional OET can only operate in media with low-conductivity (<0.01 to 0.1 S/m). Typical cell culture media or physiological buffers have significantly higher conductivities of approximately 1.4 S/m. Thus, to manipulate mammalian cells in conventional OET devices, the salts in cell culture media are replaced by osmotically equivalent amounts of non-electrolytes. This technique allows short-term sustainment of cell viability. In low-conductivity buffers, OET manipulation of cells has been demonstrated for various cell types, including human B cells,[1] yeast,[25] red and white blood cells,[11] Jurkat and HeLa cells,[12] and motile protozoan cells.[26] Nonetheless, these solutions are non-physiological, and cells lose their normal functions, such as proliferation and growth, in such media.[27] In

[a]*University of California–Berkeley, Berkeley Sensor and Actuator Center, Department of Electrical Engineering and Computer science, 476 Cory Hall, Berkeley, CA, 94720, USA. E-mail: hsu@eecs.berkeley.edu; Tel: +1-510-642-1023*
[b]*Currently at the University of Hawaii at Manoa, Department of Electrical Engineering, 2540 Dole Street, Honolulu, HI, 96822, USA. E-mail: aohta@hawaii.edu*
[c]*Currently at University of California–Los Angeles, Department of Mechanical and Aerospace Engineering, 420 Westwood Plaza, Eng. IV, 37-138, Los Angeles, CA, 90095-1597, USA. E-mail: pychiou@seas.ucla.edu; Tel: +1-310-825-8620*

† Electronic supplementary information (ESI) available: Supplementary videos S1–S5. See DOI: 10.1039/b906593h

low conductivity buffers, cells also experience additional unspecific stress, and lose viability over time. This has been a major limitation of conventional OET for biological applications.

In this paper, we present a novel phototransistor-based OET (Ph-OET) device that enables cell manipulation in cell culture media and physiological buffer solutions. The phototransistors offers 500× higher photo-conductivity than amorphous silicon. They can be turned ON with a light intensity as low as 1 W/cm$^2$. The design, simulation, fabrication, and experimental characterization of the Ph-OET will be described. The Ph-OET has been successfully used to trap HeLa and Jurkat cells in Phosphate Buffered Saline (PBS) and Dulbecco's Modified Eagle's Medium (DMEM), two widely used media. A maximum cell transport speed of 33 μm/s was achieved, indicating a maximum force of 14.5 pN. Using dynamic optical images generated by a digital light projector, we have demonstrated local concentration of cells and individually addressable cell arrays.

## Principle of phototransistor-based OET

The principle of Ph-OET is illustrated in Fig. 1. The Ph-OET device consists of sandwiched layers of a transparent indium-tin-oxide (ITO) electrode, liquid media, a pixelated phototransistor array, and a bottom electrode. An alternating current (AC) bias is applied between the top and bottom electrodes. The system can be modeled as two electrically resistive elements connected in series, where one element represents the impedance of the media, and the other element represents the phototransistor impedance. Without light, the phototransistor has the higher impedance, and it is in the OFF state. Most of the voltage drops across the phototransistor, and the electric field in the liquid is very weak. The phototransistor can be switched ON by light, as its impedance drops in the presence of light. In the ON state, it becomes a "virtual electrode", producing a non-uniform electric field around the pixel to interact with cells through DEP.

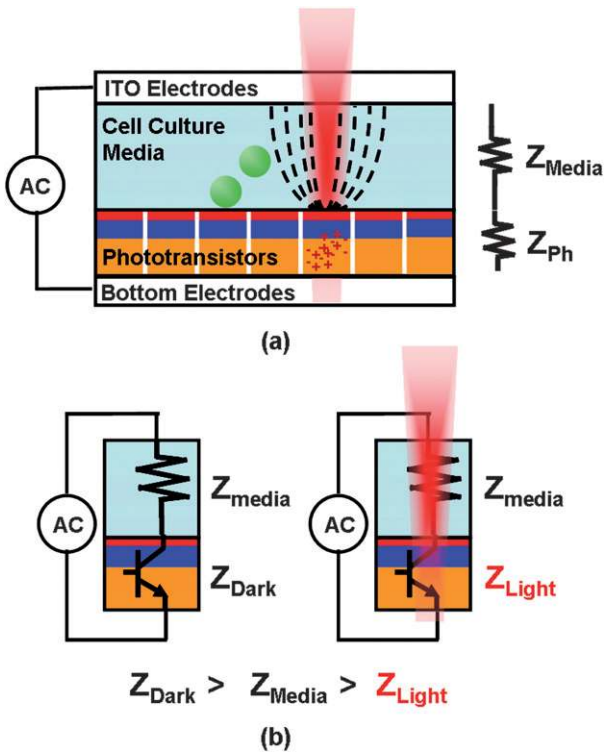


**Fig. 1** **(a)** Operating principle of the Ph-OET device. The device consists of a top ITO electrode, the cell culture media, a phototransistor array, and a bottom electrode. When light is projected onto one phototransistor, it switches the phototransistor ON, and generates an electric field locally in the media. The non-uniform electric field then exerts DEP force on the particles or cells. **(b)** Impedance comparisons between phototransistors and the media. In dark, the phototransistors are in OFF state, and their impedance is higher than the impedance of the media. With light, the phototransistors are switched ON, and their impedance becomes lower than the media impedance.

### Phototransistor design

Bipolar junction phototransistors provide a high photo-conductance and a low dark conductance. Typical NPN phototransistors are built with highly n-doped emitters, moderately p-doped bases, and lightly n-doped collector regions. In the dark, the phototransistors are in the OFF state and provide no current. Under illumination, photons absorbed in the base-collector reverse-biased junction generate an effective base current, which is further amplified by the phototransistor gain.

The two important parameters of the phototransistor are the photo-conductivity and dark-conductivity. For Ph-OET, it is desirable to obtain a photo-conductivity that is ten times higher than the liquid conductivity, while the dark-conductivity should be ten times lower. The photo- and dark-conductivities can be tuned by varying the doping profile. To find the optimal doping profile, Medici device simulation software (Synopsys, Inc.) was used to simulate the photo- and dark-conductivities with various base and emitter doping concentrations. The simulation assumes an emitter thickness of 150 nm, a base thickness of 500 nm, a collector doping concentration of $6 \times 10^{14}$ cm$^{-3}$, and an optical intensity of 1 W/cm$^2$ at a wavelength of 633 nm.

The simulated photo- and dark-conductivities are shown in Fig. 2a and 2b, respectively. The photo-conductivity is highest with high emitter doping and low base doping. On the other hand, the dark-conductivity is primarily a function of base doping. It increases dramatically when the base doping is below $3 \times 10^{16}$ cm$^{-3}$. Therefore, a high emitter doping on the order of $10^{19}$ cm$^{-3}$ and a moderate base doping of approximately $3 \times 10^{16}$ cm$^{-3}$ is most desirable.

## Fabrication and characterization

The phototransistor arrays are fabricated on a highly n-doped silicon substrate with a 5-μm thick, n-doped epitaxial layer with a resistivity of 5 to 10 Ω-cm. Fig. 3a shows the Ph-OET fabrication process. The n$^+$-p-n profile is created by two ion implantations. Boron was implanted first with a dosage of $2 \times 10^{12}$ cm$^{-2}$ and an energy of 20 keV. It is followed by a drive-in step at 1000 °C in a furnace for 90 minutes. Arsenic is then implanted with a dosage of $5 \times 10^{15}$ cm$^{-2}$ and an energy of 10 keV. The sample is annealed at 900 °C for 15 minutes. The doping profile of the phototransistor simulated by Tsuprem4 device processing simulation software (Synopsys, Inc.) is shown in the table in Fig. 3a. The phototransistor is physically patterned into square pixels of 10 μm × 10 μm area. The pixel size is chosen to be

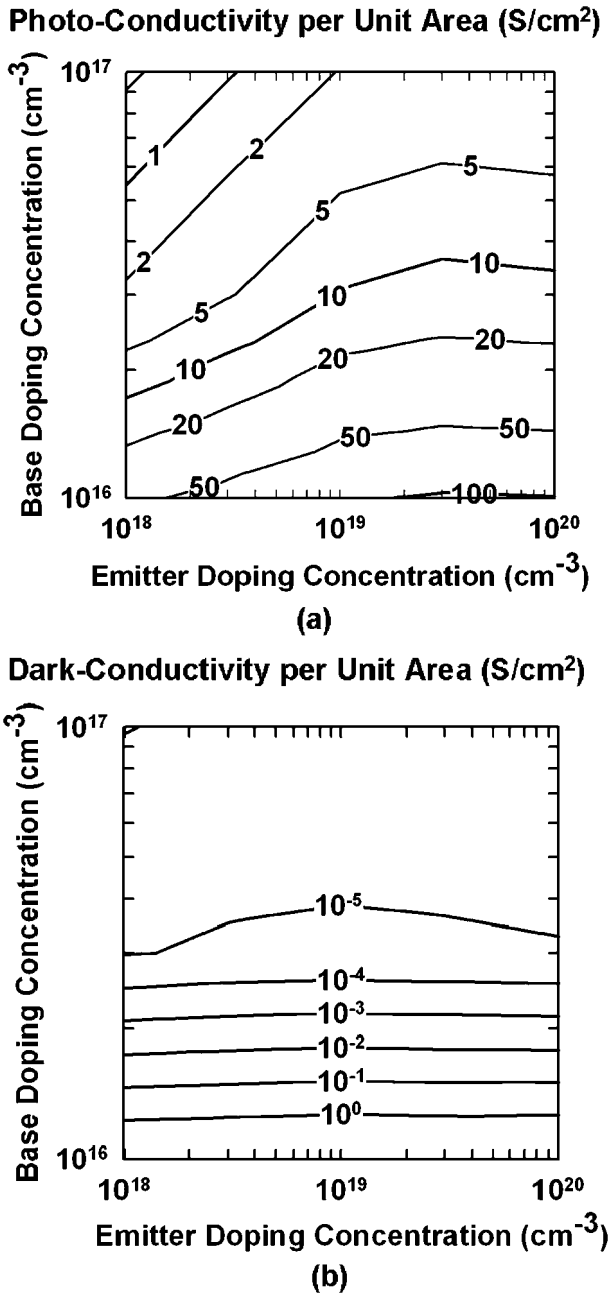


**Fig. 2** Simulated **(a)** photo-conductivity and **(b)** dark-conductivity per unit area of phototransistors as a function of base and emitter doping concentrations. A high emitter doping concentration and a low base doping concentration provides high photo-conductivity. The dark-conductivity is a strong function of base doping concentration, and it increases drastically if the base doping is lower than $3 \times 10^{16}$ cm$^{-3}$. The ideal phototransistor has high photo-conductivity while keeping dark-conductivity low. Therefore, a phototransistor with a high emitter doping ($1 \times 10^{19}$ cm$^{-3}$) and a moderate base doping ($\sim 3 \times 10^{16}$ cm$^{-3}$) is desirable.

comparable to that of mammalian cells. The pixels are isolated by reactive-ion-etched trenches (2 μm wide and 3 μm deep), which are filled with photoresist and hard baked at 120 °C for 2 hours to prevent liquid contact with the base and collector. Silicon dioxide or other dielectric materials can replace the photoresist.

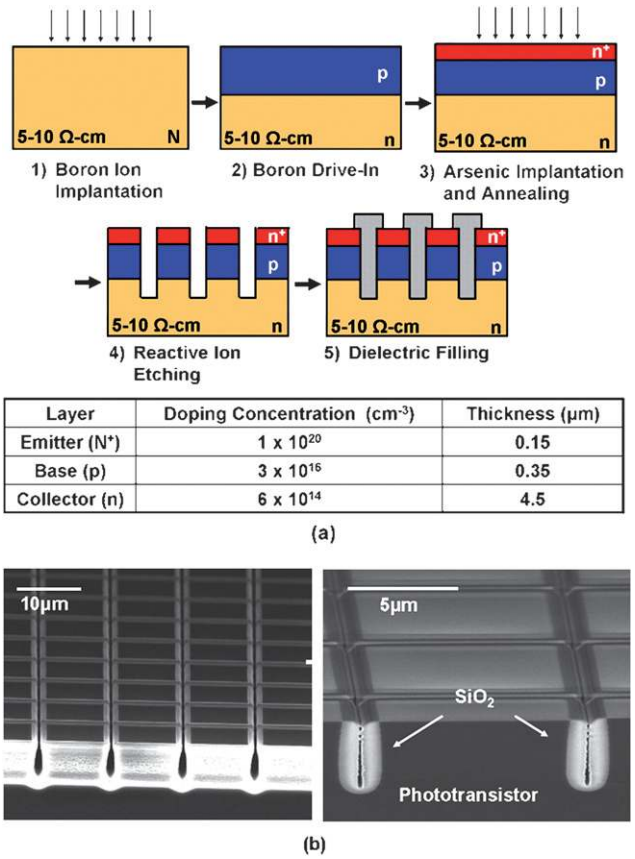


| Layer | Doping Concentration (cm$^{-3}$) | Thickness (μm) |
|---|---|---|
| Emitter (N$^+$) | $1 \times 10^{20}$ | 0.15 |
| Base (p) | $3 \times 10^{16}$ | 0.35 |
| Collector (n) | $6 \times 10^{14}$ | 4.5 |

(a)




(b)

**Fig. 3** **(a)** Fabrication process for the phototransistor array. Ion implant and dopant drive-in steps gives the desired phototransistor n$^+$-p-n doping profile as listed in the table. The phototransistors are pixelated with reactive-ion-etched trenches. Finally, the trenches are filled with dielectric materials, such as photoresist and silicon dioxide. **(b)** SEM pictures of the phototransistor arrays.

### Photo-conductivity measurement

A 100 μm × 100 μm test structure was used to compare the photo-conductivities of the phototransistor (Fig. 4a) and the amorphous silicon (Fig. 4b). The test structure is comprised of an isolated phototransistor or amorphous silicon film, spanning an area of 100 μm × 100 μm. The optical illumination is provided by a 658-nm diode laser, focused to a beam diameter of 100 μm. The current-*versus*-voltage (I–V) curves were recorded at various illumination intensities (Fig. 4c, d). Under a 5 $V_{DC}$ voltage and an illumination intensity of 1 W/cm$^2$, the phototransistor exhibits more than two orders of magnitude higher photo-conductivity than the amorphous silicon, thanks to the high phototransistor gain and the high carrier mobility in single crystal silicon.

The measured photo- and dark-conductivities per unit area are shown in Fig. 5 for both the phototransistor and the amorphous silicon. They are compared with the area-normalized conductivities of a 100-μm-thick 1.4 S/m cell culture medium and 0.01 S/m low-conductivity buffer. The phototransistor can be turned ON in cell culture media with an optical intensity of <1 W/cm$^2$. On the other hand, the amorphous silicon can only operate in low-conductivity buffers. Although it is possible for amorphous silicon to attain higher photo-conductivities using optical intensities of ~100 W/cm$^2$, these high intensities often cause other undesirable effects in

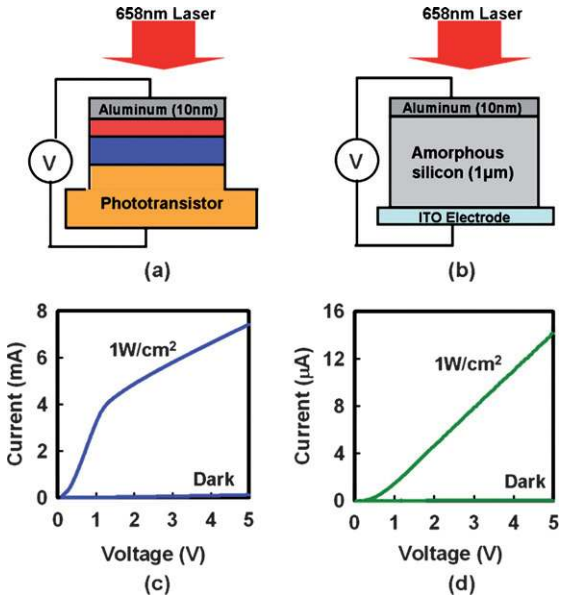


**Fig. 4** **(a–b)** Schematic of the phototransistor and amorphous silicon photoconductivity test structure. The 10-nm-thick aluminium contact has an optical absorption of 55%, which is accounted for when calculating the optical intensity. **(c–d)** Recorded I–V curves of the phototransistor and the amorphous silicon film. Under an applied voltage of 5 V and an optical illumination of 1 W/cm$^2$, the phototransistor provides a higher current (7 mA) than the amorphous silicon (0.014 mA).

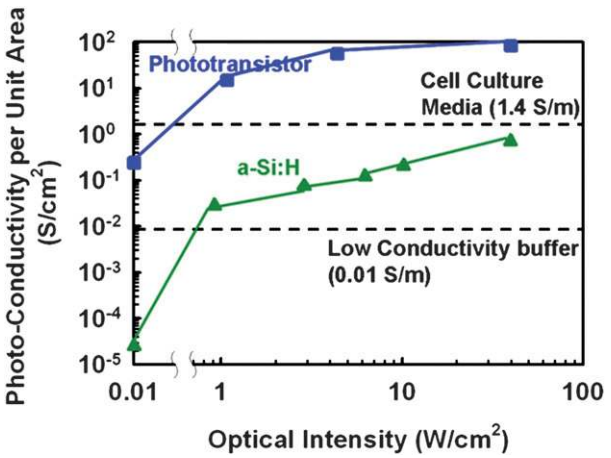


**Fig. 5** Photo-conductivity per unit area of the phototransistor and the amorphous silicon as a function of optical intensity. The phototransistor photo-conductivity can exceed the conductivity of cell culture media. The photo-conductivity of amorphous silicon only exceeds that of low-conductivity buffer. The conductivity is measured at a 5 V applied bias, and normalized to a 100 μm × 100 μm area.

OET, such as liquid flows due to thermal gradients.[28] In addition, high optical intensities can cause cell damage through optical absorption or heating effects. Therefore, Ph-OET is required for efficient OET operation in cell culture media.

## Results

To assemble the Ph-OET device (Fig. 6), an ITO-coated glass is placed opposite to the Ph-OET substrate with a 100 μm spacing,

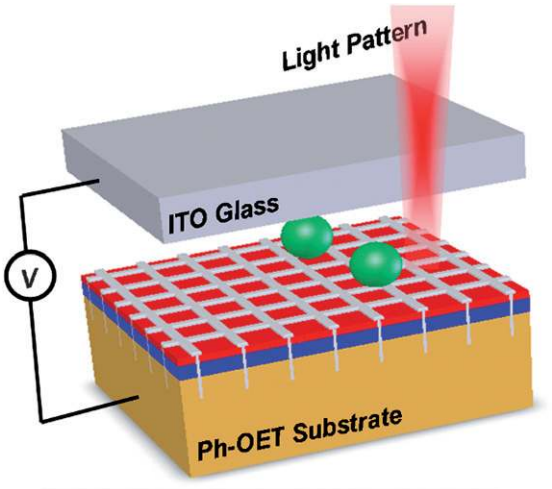


**Fig. 6** Schematic of the Ph-OET device. Samples are placed in between an ITO-coated glass and the Ph-OET. AC electric field bias is applied between the top ITO electrode and bottom silicon substrate. Optical access is provided through the ITO glass.

forming a micro-fluidic chamber. Cell and particle suspensions are introduced into the chamber. An AC voltage bias is applied between the top ITO electrode and the bottom silicon substrate. Optical access, for both observation and optical actuation, was provided through the ITO-coated glass.

### Manipulation of polystyrene beads and cells

In the Ph-OET device, the high electric field regions correspond to the optical patterns. When the optical pattern approaches the cells, it generates a negative DEP force[29] and repels the cells away. Fig. 7 shows three captured images of HeLa cells moved by optical line scans across the field of view (also supplementary video 1†). The HeLa cells were pushed against the light, and were transported from left to right by the scanning pattern. Although the phototransistor is pixelated, there is no need for the optical pattern to be aligned with the pixels.

The performance of the Ph-OET device was characterized using polystyrene beads in PBS solutions. Polystyrene beads have a constant Clausius-Mossotti (CM) factor of −0.5 for nearly all electrical bias frequencies. Therefore, for a given particle size, the actuation force is only proportional to the gradient of the square of the electric field. In these experiments, polystyrene beads with a diameter of 15 μm were suspended in

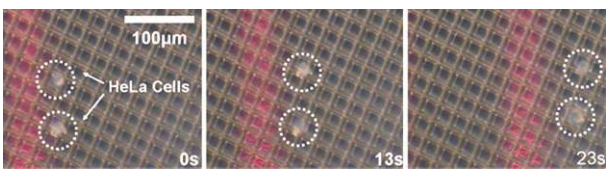


**Fig. 7** Images of cells transported across the field of view. A line-shaped optical pattern pushed the HeLa cells as it scans from left to right. Each pixelated phototransistor has an area of 20 μm × 20 μm, with 2 μm isolation gaps. The applied voltage was 20 $V_{pp}$. The grid background pattern is the phototransistor arrays; the red vertical line is the optical pattern.

a PBS solution with a conductivity of 1.4 S/m. 2 μL of the sample solution was introduced into the Ph-OET device. The applied voltage is supplied by a function generator (HP 33110A). A line-shaped optical pattern was formed with a cylindrical lens, and focused with a 20× objective lens to a spot size of 50 μm × 250 μm. A tunable neutral density filter was used to vary the optical intensity. A motorized stage (Newport) was used to move the Ph-OET device at a constant speed in a direction perpendicular to the optical pattern. The velocity of the polystyrene particles movement was measured as a function of optical intensity and electrical frequency.

The result (Fig. 8) shows that the particle velocity increases with higher optical intensity, until saturating at 13 W/cm$^2$. The saturation occurs when the virtual electrode is completely turned ON and all applied voltage is in the media; additional optical power does not effect the electric field. The Ph-OET device operates at frequencies from 1 to 9 MHz, with the most optimal performance occurring at 9 MHz. The lower velocities at low frequencies can be attributed to the screening of the electric field by the electric double layer and the native oxide layer on the silicon surface. A maximum velocity of 53 μm/s was observed with an optical intensity of 27 W/cm$^2$ and an applied voltage of 20 $V_{pp}$ at 9 MHz. This velocity is comparable to the velocity attainable with traditional OET. The Ph-OET performance is only affected by the conductivity of the liquid media; DMEM and PBS has the same electrical conductivity of 1.4 S/m, and identical results were obtained when PBS is replaced by DMEM. Therefore, Ph-OET is compatible with other types of cell culture media and saline solution with similar conductivity.

The manipulation speed of HeLa and Jurkat cells were characterized using the same experimental setup as in the polystyrene bead experiments. Cultured cells were trypsinized and resuspended in PBS solution before being introduced into the Ph-OET chamber. In these experiments, the applied frequency was fixed at 9 MHz, while the optical intensity and applied voltage were varied. The actuation velocity increases with higher applied voltage (Fig. 9a). The velocity also increases with higher optical intensity, and saturates after 13 W/cm$^2$ (Fig. 9b). The maximum cell velocity observed was 33 μm/s with an applied voltage of 20 $V_{pp}$ and an optical intensity of 10 W/cm$^2$. The velocity of

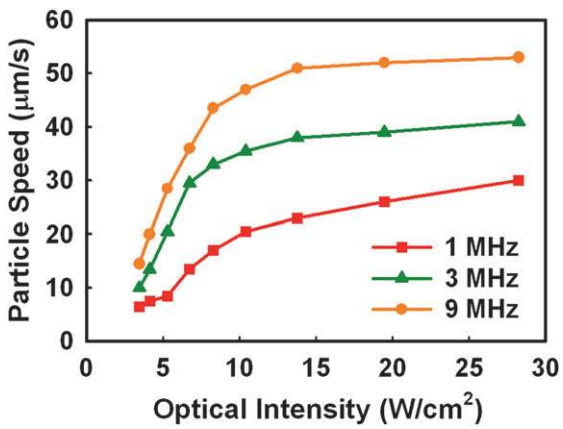


**Fig. 8** Manipulation speed of 15 μm polystyrene particles in PBS with different electric field frequency and optical intensity. The applied voltage is kept constant at 20 $V_{pp}$.

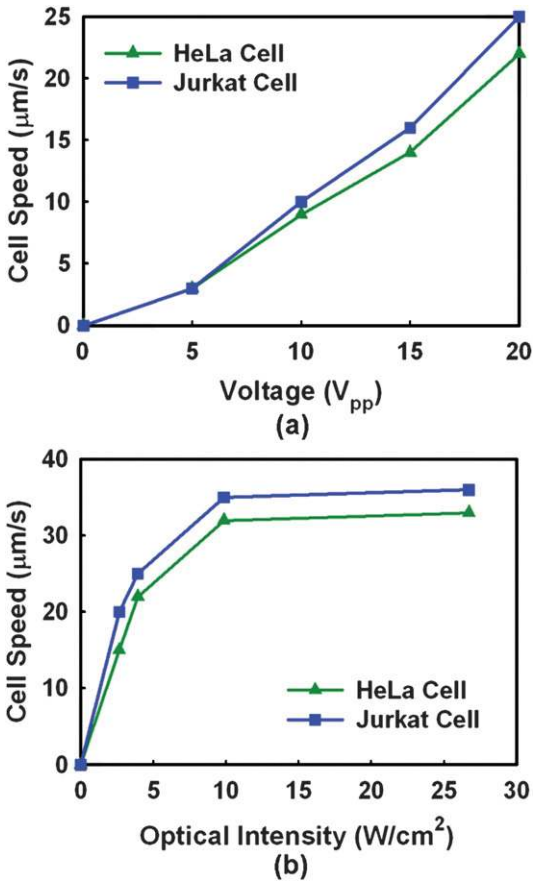


**Fig. 9** **(a)** Manipulation speed of HeLa and Jurkat cells as a function of optical intensity. The applied voltage was 20 $V_{pp}$. **(b)** Manipulation speed of HeLa and Jurkat cells as a function of voltage. The optical intensity is 4 W/cm$^2$. The applied frequency was fixed at 9 MHz for both experiments.

Jurkat cells was slightly higher than the velocities of HeLa cells due to differences in electrical properties and sizes.

The velocity measurement can be translated into the DEP force using the drag force formula with Faxen's correction:[30]

$$F = \frac{6\pi r\eta v}{\left[1 - \frac{9}{16}\left(\frac{r}{h}\right) + \frac{1}{8}\left(\frac{r}{h}\right)^3 - \frac{45}{256}\left(\frac{r}{h}\right)^4 - \frac{1}{16}\left(\frac{r}{h}\right)^5\right]}$$

where $r$ is the radius of the cell, $\eta$ is the viscosity, $v$ is the velocity, and $h$ is the distance from the device surface to the center of the cell. Using this formula, the maximum velocity of 33 μm/s corresponds to a force of 14.5 pN. This force is not able to overcome the cell adhesion, and anti-adhesion surface coating can be applied to keep cells as suspension particles.

Having an electric field in a highly conductive solution is well known to cause joule heating, which could cause a significant rise of temperature.[31] When the temperature rises above 37 °C, adverse effects such as cell death can occur. In Ph-OET device geometry, silicon substrate directly contacts the liquid layer. Single crystalline silicon has a high thermal conductivity of 148 W/m-k, which is 100× higher than that of the glass. Its high thermal conductivity makes silicon a good heat sink, and reduces

the temperature rise caused by joule heating. In an hour-long experiment under typical operating parameters, there was no loss of cell viability observed. This is tested by the exclusion of trypsin or propidium iodide dyes when added in PBS during the experiment. The effect of Ph-OET on cells over longer period of time, such as in cell culturing experiments, is currently under investigation.

### Dynamic cell manipulation

Dynamic optical patterns can be generated using a programmable digital micro-mirror device (DMD) spatial light modulator (Texas Instruments). The DMD was illuminated by a 658-nm diode laser (Newport) with a beam that was expanded by 10 times. The images from the DMD were focused onto the Ph-OET device surface with a 10× objective lens. Samples were observed using a CCD camera on a reflective microscope with dark field illumination.

Concentration of HeLa cells was demonstrated using dynamic optical patterns (Fig. 10; supplementary video 2†). We projected several concentric shrinking ring patterns onto the Ph-OET. The ring patterns collected the cells toward the center of the circles. As a result, randomly scattered cells were concentrated into the center of the rings, forming a cells aggregate.

It is straightforward to form individual addressable cell arrays using Ph-OET. We have developed a real-time user-controlled interface for the DMD. Dynamic ring patterns can be generated on demand to enclose cells. The trapped cells can then be transported and arranged into regular arrays. To demonstrate this process, a 2 × 3 array of cells was arranged (Fig. 11; supplementary video 3†). A larger 4 × 4 cell array is also demonstrated with this method (Fig. 11d, e). This process can potentially be automated by combining the dynamic programming capability with an image recognition interface. This provides a platform for patterning of single cell arrays.

One major modification of Ph-OET compared to conventional amorphous silicon OET is the pixilation of the virtual electrodes.

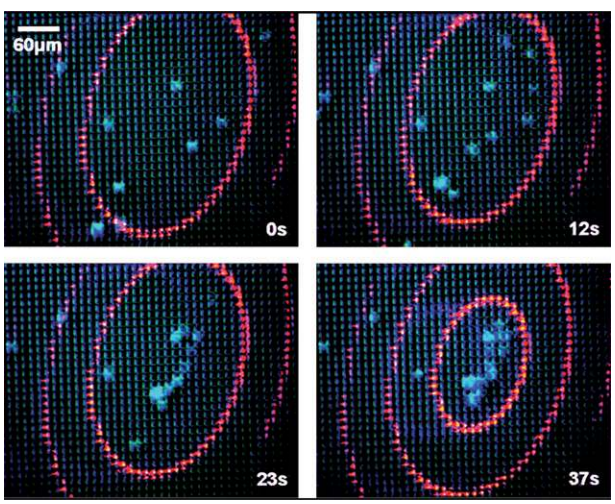


**Fig. 10** Images of local concentration of cells with dynamic optical patterns generated with DMD. Concentric optical patterns shrink and push the cells towards the center. The applied voltage was 20 $V_{pp}$ at 2 MHz frequency.

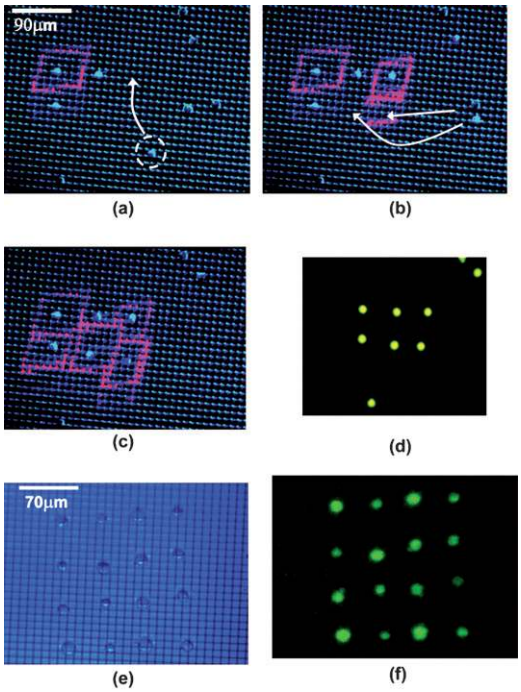


**Fig. 11** Images of an arrangement of cell arrays by user-controlled optical patterns. **(a)–(c)** Placing individual specific HeLa cells into a 2 × 3 array. The cells were trapped and transported individually by square optical pattern generated with DMD. **(d)** Fluorescent image of the assembled cell array. **(e)** Arrangement of a 4 × 4 cell array **(f)** Fluorescent image of the 4 × 4 cell array.

While conventional OET resolution is limited by the optical pattern and the amorphous silicon photo-generated charge carrier diffusion length, Ph-OET is limited by the light pattern and the phototransistor pixel size. The current Ph-OET has a pixel size of 10 μm, which is larger than the 115 nm[32] of ambipolar electron diffusion length of amorphous silicon. Though the resolution of the virtual electrode in Ph-OET is lower than the conventional OET device, particles and cells with sizes larger or comparable to the pixel size can still be trapped efficiently, as demonstrated by the trapping of a single 15 μm HeLa cell (Fig. 12a; supplementary video 4†). The cells can be stably trapped and transported by a 20 μm-wide trap bound by 10 μm-wide optical lines. The cells remain in the trap as it moves across the pixels. No alignment between optical patterns and pixels is necessary.

Quantitatively, we have characterized the trapping resolution attained with this optical pattern. Here, the resolution is defined as the maximum deviation between the geometric center of the trap and the actual cell location. This can be measured by tracking both the cell and trap central positions while optical pattern is moving laterally at a slow speed of 2.2 μm/s. The result is shown in Fig. 12b. The cell is roughly maintained at the center of the optical trap with a slight offset. The offset distance as a function of the trap position is plotted in Fig. 12c. We found the maximum cell offset from the trap center is less than 3 μm. This offset is caused by the pixelation of the phototransistor, as evidenced by the observed offset oscillation as a function of the trap center position with a 10 μm period. We expect the resolution will be sufficient for

 

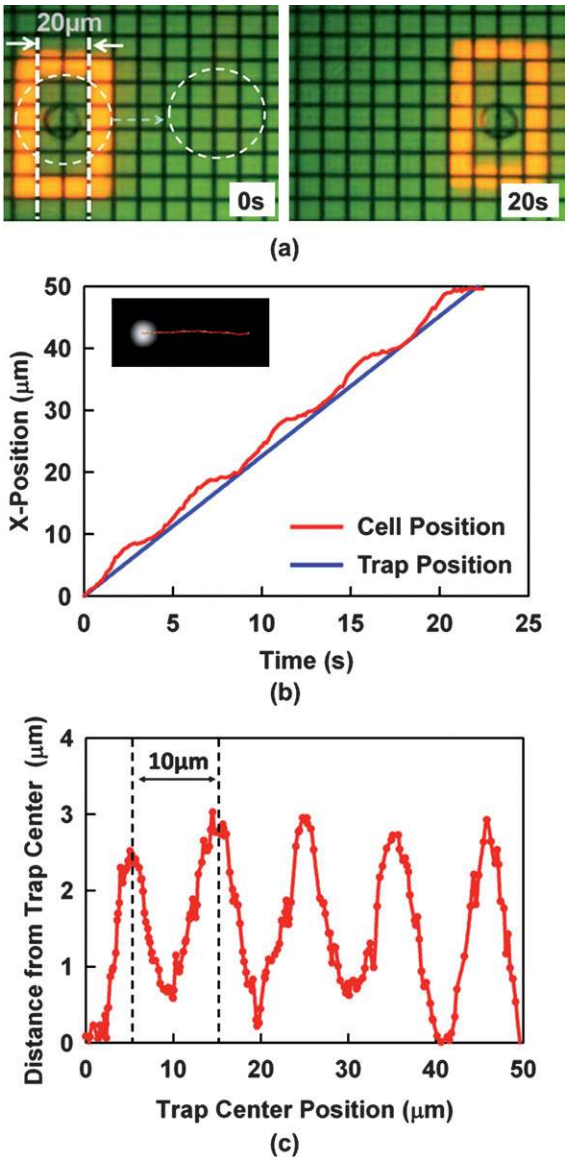


**Fig. 12** (a) Transporting of a single HeLa cell in the horizontal direction by a 20 μm-wide trap. (b) The positions of the geometric center of the trap and the cell *versus* time as the trap moves to the right. The cell's location with respect to the center of the trap varies periodically. (c) The cell-to-trap-center distance as a function of trap position.

most of the potential applications of Ph-OET. A higher resolution can be achieved with a smaller pixel size.

One potential application of Ph-OET is the investigation of cell-to-cell communication by modulating the distance between two cells. Ph-OET has the ability to control individual cells even when they are in close proximity (Fig. 13; supplementary video 5). Two cells in close contact can be separated by inserting an optical line pattern between them (Fig. 13b), and two separated cells can be joined together physically (Fig. 13c). Furthermore, some three-dimensional control is observed. When two cells were joined together in a single 20 μm square trap, they were stacked vertically (Fig. 13d, e). This is achieved by both the in-plain trapping force and the out-of-plain pearl-chaining effect that aligns the two cells vertically.

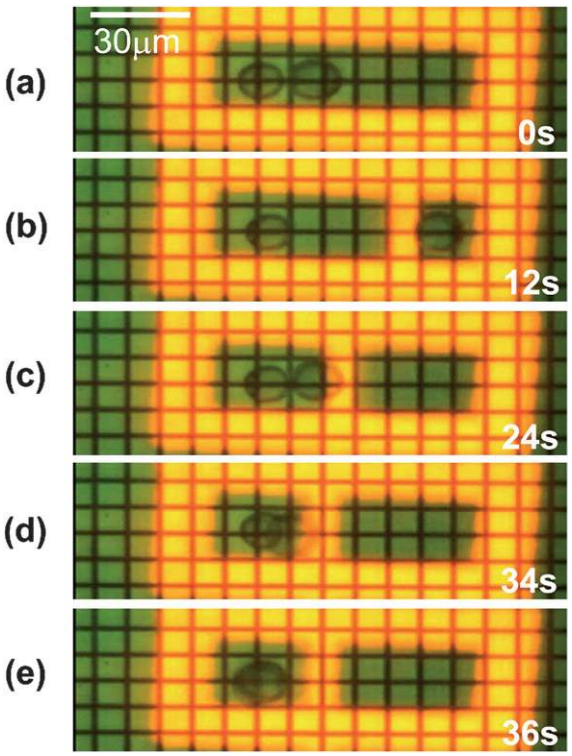


**Fig. 13** Spatial control of two cells. **(a)** Initially, two cells in close proximity are trapped in a single optical box. **(b)** Separation of the two adjacent cells. **(c)** Joining of two separated cells. **(d–e)** Stacking of 2 cells vertically in one single trap.

## Conclusion

We have demonstrated a novel phototransistor-based optoelectronic tweezers (Ph-OET) device capable of dynamic, optically-controlled single cell manipulation in cell culture media and physiological buffers. The Ph-OET provides the crucial ability to operate in cell culture media, while retaining the advantage of standard OET. This is achieved by replacing the amorphous silicon photoconductors in conventional OET by phototransistors, which enhances the photo-conductivity by more than two orders of magnitude. A Ph-OET device removes the key roadblock in biological applications of OET. The potential applications of Ph-OET include single cell array assay for drug screening, study of cell-to-cell communication, and cell sorting.

## Acknowledgements

This project is funded by National Institute of Health (NIH) through the Center for Cell Control, Grant # PN2 EY018228. The authors would like to thank the UC Berkeley Tissue Culture facility for providing cell samples. We also thank the staff of the Microfabrication Laboratory at the University of California, Berkeley for assistance with device fabrication.

## References

1 P. Y. Chiou, A. T. Ohta and M. C. Wu, *Nature*, 2005, **436**, 370–372.
2 D. G. Grier, *Nature*, 2003, **424**, 810–816.
3 A. Ashkin, J. M. Dziedzic and T. Yamane, *Nature*, 1987, **330**, 769–771.

4 R. Pethig, *Critical Reviews in Biotechnology*, 1996, **16**, 331–348.
5 P. Gascoyne, C. Mahidol, M. Ruchirawat, J. Satayavivad, P. Watcharasit and F. F. Becker, *Lab Chip*, 2002, **2**, 70–75.
6 M. P. Hughes, *Electrophoresis*, 2002, **23**, 2569–2582.
7 L. Wang, L. A. Flanagan, N. L. Jeon, E. Monuki and A. P. Lee, *Lab Chip*, 2007, **7**, 1114–1120.
8 K. Konig, H. Liang, M. W. Berns and B. J. Tromberg, *Opt. Lett.*, 1996, **21**, 1090–1092.
9 S. K. Mohanty, A. Rapp, S. Monajembashi, P. K. Gupta and K. O. Greulich, *Radiat. Res.*, 2002, **157**, 378–385.
10 H. Glasser and G. Fuhr, *Bioelectrochem. Bioenerg.*, 1998, **47**, 301–310.
11 A. T. Ohta, P. Y. Chiou, T. H. Han, J. C. Liao, U. Bhardwaj, E. R. B. McCabe, F. Yu, R. Sun and M. C. Wu, *J. Microelectromech. Syst.*, 2007, **16**, 491–499.
12 A. T. Ohta, P.-Y. Chiou, H. L. Phan, S. W. Sherwood, J. M. Yang, A. N. K. Lau, H.-Y. Hsu, A. Jamshidi and M. C. Wu, *IEEE J. Sel. Top. Quantum Electron.*, 2007, **13**, 235–243.
13 A. Jamshidi, P. J. Pauzauskie, P. J. Schuck, A. T. Ohta, P. Y. Chiou, J. Chou, P. D. Yang and M. C. Wu, *Nat. Photonics*, 2008, **2**, 86–89.
14 M. Hoeb, J. O. Radler, S. Klein, M. Stutzmann and M. S. Brandt, *Biophys. J.*, 2007, **93**, 1032–1038.
15 C. Pei-Yu, A. T. Ohta, A. Jamshidi, H. Hsin-Yi and M. C. Wu, *J. Microelectromech. Syst.*, 2008, **17**, 525.
16 A. T. Ohta, A. Jamshidi, P. J. Pauzauskie, H. Hsan-Yin, Y. Peidong and M. C. Wu, CLEO '07. 2007 *Conference on Lasers and Electro-Optics*. IEEE. pp. 828–9. Piscataway, NJ, USA.
17 A. T. Ohta, S. L. Neale, H. Hsan-Yin, J. K. Valley and M. C. Wu, 2008 *IEEE/LEOS Internationall Conference on Optical MEMs and Nanophotonics*. IEEE. pp. 7–8. Piscataway, NJ, USA.
18 M.-C. Tien, Aaron T. Ohta, Kyoungsik Yu, Steven L. Neale and Ming C. Wu, *Appl. Phys. A: Mater. Sci. Process.*, 2009, **95**, 967–972.
19 H. Hwang, Y. Oh, J. J. Kim, W. Choi, S. H. Kim, J. Jang and J. K. Park, *Biochip J.*, 2007, **1**, 234–240.
20 S. Park, C. Pan, T. H. Wu, C. Kloss, S. Kalim, C. E. Callahan, M. Teitell and E. P. Y. Chiou, *Appl. Phys. Lett.*, 2008, **92**, 151101.
21 W. Choi, S. H. Kim, J. Jang and J. K. Park, *Microfluid. Nanofluid.*, 2007, **3**, 217–225.
22 H. Hwang, Y. J. Choi, W. Choi, S. H. Kim, J. Jang and J. K. Park, *Electrophoresis*, 2008, **29**, 1203–1212.
23 J. K. Valley, S. Neale, H. Y. Hsu, A. T. Ohta, A. Jamshidi and M. C. Wu, *Lab Chip*, 2009, **9**, 1714–1720.
24 Y. H. Lin and G. B. Lee, *Appl. Phys. Lett.*, 2009, **94**, 033901.
25 Y. S. Lu, Y. P. Huang, J. A. Yeh, C. Lee and Y. H. Chang, *Opt. Quantum Electron.*, 2005, **37**, 1385–1395.
26 W. Choi, S. W. Nam, H. Hwang, S. Park and J. K. Park, *Appl. Phys. Lett.*, 2008, **93**, 143901.
27 J. Voldman, *Annu. Rev. Biomed. Eng.*, 2006, **8**, 425–454.
28 J. K. Valley, J. K. Valley, A. Jamshidi, A. T. Ohta, H. Y. A. H. H. Y. Hsu and M. C. A. W. M. C. Wu, *J. Microelectromech. Syst.*, 2008, **17**, 342.
29 G. Fuhr, H. Glasser, T. Muller and T. Schnelle, *Biochim. Biophys. Acta, Gen. Subj.*, 1994, **1201**, 353–360.
30 K. Svoboda and S. M. Block, *Annu. Rev. Biophys. Biomol. Struct.*, 1994, **23**, 247–285.
31 U. Seger-Sauli, M. Panayiotou, S. Schnydrig, M. Jordan and P. Renaud, *Electrophoresis*, 2005, **26**, 2239–2246.
32 R. Schwarz, F. Wang and M. Reissner, *Appl. Phys. Lett.*, 1993, **63**, 1083–1085.


 